Supporting Information. Elahi, R., Edmunds, P.J., Gates, R.D., Kuffner, I.B., Barnes, B.B., Chollett, I., Courtney, T.A., Guest, J.R., Lenz, E.A., Toth, L.T., Viehman, T.S., Williams, I.D. 2022. Scale dependence of coral reef oases and their environmental correlates. Ecological Applications.

Appendix S1.

Any use of trade, firm, or product names is for descriptive purposes only and does not imply endorsement by the U.S. Government.

Section S1. Supporting Methods

Defining spatiotemporal vs spatial oases

We used time-series data from our previous analysis of spatiotemporal oases (Guest et al. 2018) to examine the sensitivity of oasis designation to temporal replication. How many years of data do we need to eliminate errors in designating a given reef site as an oasis? And conversely, what is the error rate when we have only one year of data? The latter question is directly relevant to the spatial analysis we present in this paper. We consider the oases identified from the complete time-series (Guest et al. 2018) as the most accurate designation because they are based on 11 to 24 years of data for each of four regions (Florida Keys, US Virgin Islands, main Hawaiian Islands, and French Polynesia).

We used simulations to examine the consequence of varying the number of years available for analysis. Each simulation consisted of drawing a random number (i) of years from the complete time-series in each region, and then designating each reef site as an oasis or not, based on the proportion of occasions where a site exhibited coral cover two standard deviations above its regional mean value (i.e., z-score > 2). Whereas Guest et al. (2018) considered any site that had a positive z-score to be a potential spatiotemporal oasis, we used two standard deviations in our simulations because this was the threshold used to assign spatial oases in the current study. For each set of simulations (n = 1,000) with a given number of years i, we calculated the percent of true/false positives and negatives, with corresponding quartiles. For example, a true positive correctly identifies an oasis (i.e., sensitivity), and a false positive misidentifies a site as an oasis. Even with only one year of data, false positive error rates were minimal (0 – 5%) and true oases were always identified correctly (i.e., sensitivity was 100%) for the US Virgin Islands, main Hawaiian Islands, and French Polynesia, (Fig. S1), suggesting that the assignment of oases with the stricter criteria used in this study was robust to subsampling. However, error rates were considerable for the Florida Keys, with sensitivity ranging between 70 and 100%. These misidentifications may be due to the fact that the Florida Keys have been subjected to many and diverse disturbances over the past few decades (e.g., cold-water intrusions, bleaching, disease; Courtney et al. 2020). More disturbances would result in greater variability in coral cover, and thus a higher error rate in oasis designations based on one or only a few years of data. Considering that our current analysis relies on recent data (2012 – 2017; Fig. S2), after decades of coral decline, we consider the designation of spatial oases using our highly-replicated dataset to be reasonably robust to errors arising from frequent disturbances.

Coral reef data

We used data collected by the United States National Oceanic and Atmospheric Administration (NOAA) Coral Reef Conservation Program's (CCRP) National Coral Reef Monitoring Program (NCRMP) which monitors reefs in the Pacific and Atlantic Oceans (https://www.coris.noaa.gov/monitoring/). Data on benthic cover in the Pacific Ocean were collected between 2012 and 2017 by the Coral Reef Ecosystem Program of NOAA's Pacific Island Fisheries Science Center. At each randomly selected reef site (McCoy et al. 2016), a digital camera (Canon PowerShot S110, 12.1 megapixel) recorded an area of 0.7 m^2 of the benthos at 1 m intervals along a 30 m transect line (30 photographs $site^{-1}$). These photographs were analyzed using stratified-random point counts (10 points $photograph^{-1}$) to estimate the percentage cover of coral species and genera, as well as other benthic groups (Williams et al.

2019). Data on benthic cover in the western Atlantic (Florida, Puerto Rico, and the U.S. Virgin Islands) were collected between 2013 and 2017 by NOAA's NCRMP program and partners. Regions were sampled every two years. A grid-based stratified random design was used to select sample locations. Line-point-intercept transects (15 m in length) were used to estimate benthic cover to the lowest possible taxonomic resolution (scleractinian corals, as well as calcified octocorals and hydrozoan corals), functional group (other benthic organisms), or substratum type. For the purposes of our analyses, we summed the total percentage cover of calcifying corals as our response variable. We acknowledge that using total percent cover may mask important dynamics of coral functional groups or taxa (Nyström 2006, Darling et al. 2019) or population demographics (Hughes 1996, Edmunds and Elahi 2007), but it does correlate well with one measure of a reef community's ability to produce calcium carbonate structures (coral calcification capacity; Guest et al. 2018). Here, we use total cover as an aggregate metric of coral reef condition to illustrate our modeling approach to identifying the correlates of oases, but the approach can be extended to any continuous metric that can be used to assign a binary categorization of oasis / not oasis.

Environmental predictors of coral reef oases

To determine which environmental features were associated with the occurrence of coral oases, we compiled remote sensing data from several sources. We selected predictors hypothesized to influence coral cover from macroecological (> 1000 km) to local scales (< 1 km), including abiotic and socioeconomic covariates. We used the Marine Socio-Environmental Covariates (MSEC) dataset to obtain net primary productivity, wave energy, land area, and human population density (Yeager et al. 2017). We also derived sea-surface temperature, light attenuation in the water column, and storm activity from other published databases (Table S2). These variables were chosen due to previously demonstrated associations with coral cover (e.g., Williams et al. 2015, Darling et al. 2019), or hypothesized relationships based on mechanistic biological understanding (e.g., through laboratory experiments). In addition to using a measure of central tendency (i.e., the mean) for primary productivity, temperature, light attenuation, and wave exposure, we also considered a measure of variability (i.e., coefficient of variation; CV). With the mean and CV, we were able to characterize the physical regime in as few parameters as possible. We did not include depth as a covariate because a statistical analysis demonstrated no relationship ($\chi^2 = 0.002$, $P = 0.97$) between coral cover and depth at each site. That is, we compared a linear mixed-effects model (random intercepts of sub-jurisdiction) with a coefficient for depth to a null model with only an intercept term. We also visualized the relationship between coral cover and depth for each jurisdiction in Fig. S3. The extent to which relationships between environmental covariates and oasis occurrence changes with spatial extent is unclear, and we describe some of our expectations below.

Temperature. Sea-surface temperature (SST) was obtained from the National Aeronautics and Space Administration (NASA). For each site, we extracted the mean and variance of monthly mean products of SST to characterize the thermal environment in as few parameters as possible. Specifically, level-3 BIN monthly composites (Jan 2003 – Dec 2017) of MODIS SST (nighttime 4µm) acquired from NASA OBPG archives (https://oceancolor.gsfc.nasa.gov/cgi/l3). These were mapped using the SeaDAS (version 7.4) routine l3mapgen to a cylindrical equidistant projection with 2.5 arcminute resolution and boundaries of 15S – 29N, 144E – 64W (longitude 0 = 180). Cubic interpolation was used to fill gaps in the data, which resulted primarily from land and persistently cloudy conditions in equatorial Pacific regions. Pixels identified as land (according to the GSHHS version 2.3.7 "high" resolution landmask, mapped to the same projection as above; Wessel and Smith 1996) were removed. The mean and variance was derived from the calculated monthly mean SST. Although it would have been useful to obtain an estimate of higher frequency temperature variability, as corals may benefit from exposure to large thermal fluctuations on daily to weekly scales (e.g., Safaie et al. 2018), we chose to calculate summary statistics using monthly means because of the highly variable number of satellite observations per grid cell over shorter timescales due to cloudy conditions. Moreover, our monthly estimates of SST mean and variance were highly correlated ($r > 0.98$) with weekly estimates from the global Coral Reef Temperature Anomaly Database (CoRTAD Version 5) from the National Oceanic and Atmospheric Administration (www.nodc.noaa.gov/sog/cortad/). We standardized the metric of variability using the coefficient of variation (CV) by squaring the variance and dividing by the mean. At macroecological scales, coral cover in the central-western Pacific was positively associated with average SST (Williams et al. 2015) and average minimum SST (Robinson et al. 2018), consistent with the global distribution of coral reefs in tropical waters. Therefore, we expected a positive association between coral oases and mean SST at macroecological scales, but variable associations at local scales depending on the prevalence of adaptation or acclimatization to ‘hot spots’ at finer management scales due to variation in water flow and residence time (Craig et al. 2001, Oliver and Palumbi 2011, Palumbi et al. 2014). Similarly, long-term variability in temperature may precondition corals to thermal anomalies and reduce bleaching (Sully et al. 2019), and thus we expected a positive association between coral oases and the CV of temperature, but the consistency of this expectation across spatial extents was unclear.

Light attenuation. Light attenuation (quantified as the diffuse attenuation coefficient for downwelling irradiance at 490nm; K_d490 in m^{-1}) was obtained from the National Aeronautics and Space Administration (NASA) (Barnes et al. 2013). Higher values of K_d490 represented greater light attenuation and thus lower water clarity and vice versa. Light attenuation, as measured by K_d490, includes suspended particles (which both absorb and scatter light) and dissolved organic matter (DOM; which only absorbs light). In contrast, turbidity describes particles and not DOM, and thus we do not use the term turbidity to describe K_d490 (e.g., Sully and van Woesik 2020). For each site, we extracted the mean and variance of K_d490 to characterize the light environment in as few parameters as possible. Specifically, level-3 BIN monthly composites (Jan 2003 – Dec 2017) of K_d490 (as derived using the KD2 algorithm) acquired from NASA OBPG archives (https://oceancolor.gsfc.nasa.gov/cgi/l3). These were mapped using the SeaDAS (version 7.4) routine l3mapgen to a cylindrical equidistant projection with 2.5 arcminute resolution and boundaries of 15S – 29N, 144E – 64W (longitude 0 = 180). Cubic interpolation was used to fill gaps in the data, which resulted primarily from land and persistently cloudy conditions in equatorial Pacific regions. Pixels identified as land (according to the GSHHS "high" resolution landmask, mapped to the same projection as above) were removed. The mean and variance was derived from the monthly mean K_d490, which was particularly important because seasonal variation (i.e., fewer during cloudy summer months) in the number of satellite observations precluded the use of a finer temporal resolution (e.g., weekly estimates of K_d490). As with SST, we used CV as a standardized estimate of variability in K_d490 by squaring the variance and dividing by the mean. Due to the fact that high irradiance can exacerbate temperature-related bleaching in corals (Lesser et al. 1990), protection from high light, through cloud cover or productive nearshore waters, can ameliorate coral bleaching associated with exceptional warming events (Fitt and Warner 1995, Mumby et al. 2001). The suspension of sediment in the water column, turbidity, is another mechanism that can reduce light attenuation. Turbidity is typically considered a stressor to corals that requires specific mechanisms of adaptation (Anthony and Larcombe 2000), due to the smothering effects of sedimentation and associated reductions in available light for photosynthesis (Kleypas 1996). In summary, the remotely sensed measurement of light attenuation (K_d490) is influenced simultaneously by a number of physical and biological processes in the water column, and can have both positive and negative effects on coral physiology, especially in the context of a variable thermal environment. A global analysis demonstrated that coral bleaching was associated positively with K_d490, but associated negatively with the interaction between K_d490 and SST; whether the interaction reflected the expectation that light attenuation would be beneficial under thermally stressful conditions was not investigated (Sully and van Woesik 2020). Based on these previous case studies and synthesis, we expected a negative, or complex association (e.g., intermediate levels of light attenuation as beneficial; Sully and van Woesik 2020), between extinction coefficient K_d490 and the probability of oasis occurrence. Similarly, we expected a complex association between the CV of light attenuation and oasis occurrence. For example, higher CV indicates greater inconsistency in the detrimental effects or potential benefits of reduced irradiance. We did not have explicit hypotheses about how these relationships would change with spatial extent.

Primary productivity. Estimates of net primary productivity (NPP) in the seawater column based on NOAA CoastWatch were derived from 8-day composite layers from 2003-2013 (https://coastwatch.pfeg.noaa.gov/erddap/griddap/erdPPbfp28day.graph?productivity). NPP was modelled on a 2.5 arcminute grid based on photosynthetically available radiation, SST, and chlorophyll *a* concentration. The mean of each sampling week (8-day composite) was used for calculating the mean and standard deviation for the entire period (2003-2013). These latter two products were downloaded from the MSEC database (Yeager et al. 2017). Each site was then joined to the nearest (straight-line distance) estimate of primary productivity (i.e., centroid of the 2.5 arcminute grid cell) using the R package `fuzzyjoin` (Robinson 2019). Across the Indo-Pacific, this metric of net primary productivity was associated with lower coral cover, suggesting unfavorable conditions for corals in eutrophic areas (Darling et al. 2019). In contrast, coral cover across the central-western Pacific was associated positively with mean estimates of chlorophyll *a*, as well as anomalies in chlorophyll *a* (Williams et al. 2015, Robinson et al. 2018), interpreted to reflect beneficial effects of increased nutrient supply, either directly as an energetic subsidy to corals, or through the positive, indirect effects of herbivorous fish populations. Thus, the influence of NPP on sites vary with spatial extent.

Wave energy. Wave energy flux (the power transmitted per unit of wavefront width) at a 2.5 arcminute resolution was calculated using the WAVEWATCH III hindcast dataset (http://polar.ncep.noaa.gov/waves/CFSR_hindcast.shtml), which spanned 31 years at a 3-hour temporal resolution. Estimates of wave energy were modified at sheltered locations by considering wind speed, fetch and depth (Marchand and Gill 2017). Mean wave energy was calculated for each day, and then used for calculating mean and standard deviation for the entire period (1979-2009). These latter two products were downloaded from the MSEC database (Yeager et al. 2017). Each site was then joined to the nearest (straight-line distance) estimate of wave energy (i.e., centroid of the 2.5 arcminute grid cell) using the R package `fuzzyjoin` (Robinson 2019). At macroecological scales, coral cover is associated negatively with mean wave energy (Robinson et al. 2018, Darling et al. 2019) and the magnitude of wave anomalies (Williams et al. 2015), due to fragmentation and mortality caused by large physical disturbances. However, wave energy can also mitigate the deleterious effects of high temperature anomalies at local scales through the effects of internal waves (Wall et al. 2015, Wyatt et al. 2020), hurricanes (Manzello et al. 2007), and water flow (Nakamura and van Woesik 2001), and thus the consistency of wave energy effects across spatial extent is unclear.

Storms. Storm data were obtained from the International Best Track Archive for Climate Stewardship (IBTrACS v03r10) (Knapp et al. 2010) which merges storm information from multiple climate centers into one product with a common format. Initial dates vary according to the source agency, but all data are available from 1897 through 2016 or 2017. Data for 2017 for the North Atlantic basin (the only basin missing data with sampling that year) were complemented with data from NOAA's National Hurricane Center. We limited our study to storms at Saffir-Simpson intensity three (i.e., Category 3; sustained wind speed ≥ 96 knots) and above. Storms reaching Category 3 and higher are considered major storms because of their potential for generating waves of sufficient energy to cause significant loss of life and damage (Simpson and Saffir 1974). For each site, we calculated the number of major storms within a radius of 100 km. This area of influence reflects the grid size commonly used in storm climatological studies (Elsner et al. 2012) and encompasses potential damage from storms to coral communities observed in situ (Woodley et al. 1981, Treml et al. 1997, Puotinen 2004, Gardner et al. 2005). The frequency of major storms was calculated for 30 years before the date of site sampling to provide an estimate of storm exposure that was comparable to the duration of other metrics considered in this study. As described for 'wave energy' above, we expected that over large spatial extents, periodic cyclone impacts would have a negative impact on coral cover because of physical damage to the reef. However, hurricanes can also provide short-term relief from thermal stress (Manzello et al. 2007), which may result in a more complex relationship with coral oases at smaller spatial extents.

Land area. The total amount of land area within a 50 km radius of each site was used as a proxy for terrestrial inputs (e.g., nutrients, pollution) onto coral reefs, and was calculated using the 0.25 arcminute the global, self-consistent, hierarchical, high-resolution shoreline (GSHHS) database (Wessel and Smith 1996). This product was downloaded from the MSEC database (Yeager et al. 2017). We hypothesized that greater land area would be associated with a lower probability of oasis occurrence, if land area is indeed a proxy for negative terrestrial influences to nearshore coral reefs. The amount of rainfall and the inclination of land likely influence the flow of terrestrial subsidies into nearshore habitats, but we do not consider these characteristics in our analysis.

Human population density. The number of people within a 50 km radius of each site in 2015 was used as a proxy for human impacts on coral reefs. The population count estimates were produced by the Socioeconomic Data and Applications Center at a resolution of 0.5 arcminute. This product was downloaded from the MSEC database (Yeager et al. 2017). Human population density is typically assumed to be correlated positively with harmful impacts, including pollution, fishing, and coastal modifications. Coral cover was associated negatively with uninhabited islands in the central Pacific (Smith et al. 2016), and associated negatively with population gravity (a function of human population size and reef accessibility) (Darling et al. 2019) in the Indo-Pacific. In contrast, human population size was not associated with coral cover in a global synthesis (Bruno and Valdivia 2016), and thus the overall effect of this factor is not clear and may depend on spatial extent.

Summarizing predictors and assessing multicollinearity

Each site was associated with a 2.5 arcminute grid cell for the purposes of our statistical model. Temperature and light attenuation were estimated using the centroid of the site grid cells. For the variables that were calculated for each specific site (i.e., land area, human population density), the mean value was calculated using all the sites within a grid cell. The same was done for estimates of primary productivity and wave energy, but in this case, the mean value was the same as the individual value for each site, because the resolution of these two predictors was 2.5 arcminutes. Lastly, the total number of storms over the past 30 years was calculated as the mean across all sites within a given grid cell. The distributions of all covariates at each management scale are visualized in Figs. S4-S7.

We assessed multicollinearity among the predictors using variance inflation factors (VIF; Table S3) and Pearson correlation coefficients (r), for each scale of analysis. In general, we followed the approach suggested by Zuur et al. (2010) and removed predictors with the highest VIFs and correlation coefficients sequentially until all VIFs < 3 and $r < 0.7$, but we also considered the hypotheses being tested. Specifically, there were strong correlations ($r > 0.7$) between human population density and land use area, as well as the mean and CV of SST at several spatial extents included in our analysis. When there were strong correlations, we chose to retain population density rather than land area as an overall measure of human impacts, and we chose to retain the variability (CV) of SST rather than the mean, to test the hypotheses outlined above. However, we emphasize that these estimates will be more difficult to interpret due to their covariance with the other known predictors.

When predictors were standardized at the cross-basin and basin spatial extents, we removed land area and mean SST (Table S3). When predictors were standardized by region, we removed land area but retained both mean and CV of SST (Table S3). At the sub-regional scale, we were able to retain all the predictors (Table S3). Some sub-regions displayed no variability in the predictors and thus the standardized predictor was undefined. Therefore, we added a small (< 5% of the minimum observed value) value to human population density, storms, and land area. Due to the fact that land area was not included at the three larger spatial extents, we also chose to remove it from the sub-regional analysis. The total number of grid cells (i) was 890 across 32 sub-regions (Table S1).

Section S2: Supporting Tables

Table S1. The number of grid cells (*i*) sampled within each sub-region, nested within region and basin, used in the present analysis of oases.

Basin	Region	Sub-region	*i*
Western Atlantic	Florida	Keys-lower	34
Western Atlantic	Florida	Keys-middle	31
Western Atlantic	Florida	Keys-upper	38
Western Atlantic	Florida	Southeast Florida	41
Western Atlantic	Florida	Tortugas	51
Western Atlantic	Puerto Rico	Puerto Rico-east	46
Western Atlantic	Puerto Rico	Puerto Rico-north	21
Western Atlantic	Puerto Rico	Puerto Rico-southwest	66
Western Atlantic	US Virgin Islands	St. John	10
Western Atlantic	US Virgin Islands	St. Thomas	18
Western Atlantic	US Virgin Islands	St. J & St. T offshore	16
Western Atlantic	US Virgin Islands	St. Croix	33
Pacific	Mariana Islands	Guam	30
Pacific	Mariana Islands	Marianas-lower	24
Pacific	Mariana Islands	Marianas-middle	18
Pacific	Mariana Islands	Marianas-upper	6
Pacific	Mariana Islands	Rota	8
Pacific	Northwest Hawaiian Islands	French Frigate	30
Pacific	Northwest Hawaiian Islands	Kure	8
Pacific	Northwest Hawaiian Islands	Lisianski	16
Pacific	Northwest Hawaiian Islands	Pearl & Hermes	23
Pacific	Main Hawaiian Islands	Hawaii	74
Pacific	Main Hawaiian Islands	Kahoolawe	7
Pacific	Main Hawaiian Islands	Kauai	26
Pacific	Main Hawaiian Islands	Lanai	32
Pacific	Main Hawaiian Islands	Maui	37
Pacific	Main Hawaiian Islands	Molokai	41
Pacific	Main Hawaiian Islands	Niihau	19
Pacific	Main Hawaiian Islands	Oahu	47
Pacific	American Samoa	Manua Islands	12
Pacific	American Samoa	Rose	4
Pacific	American Samoa	Tutuila	23

Table S2. Table of predictors considered in this study.

Description	**Years**	**Units**	**Source**
Net primary productivity of carbon, mean of weekly means	2003-2013	mg C m^{-2} day^{-1}	Yeager et al. 2017
Net primary productivity of carbon, standard deviation of weekly means	2003-2013	mg C m^{-2} day^{-1}	Yeager et al. 2017
Wave energy flux, mean of weekly means	1971-2009	kW m^{-1}	Yeager et al. 2017
Wave energy flux, standard deviation of weekly means	1971-2009	kW m^{-1}	Yeager et al. 2017
Land area within a 50 km radius		km^2	Yeager et al. 2017
Human population count within a 50 km radius	2015	individuals	Yeager et al. 2017
Sea-surface temperature, mean of monthly means	2003-2017	°C	NASA OBPG archives (https://oceancolor.gsfc.nasa.gov)
Sea-surface temperature, standard deviation of monthly means	2003-2017	°C	NASA OBPG archives (https://oceancolor.gsfc.nasa.gov)
Light attenuation, mean of monthly means	2003-2017	K_d490 in m^{-1}	NASA OBPG archives (https://oceancolor.gsfc.nasa.gov)
Light attenuation, standard deviation of monthly means	2003-2017	K_d490 in m^{-1}	NASA OBPG archives (https://oceancolor.gsfc.nasa.gov)
Number of category 3, 4, 5 storms within a 100 km radius	30 years prior to site survey	count	IBTrACS v03r10, Knapp et al. 2010

Table S3. Variance inflation factors (VIF) for the final set of predictors considered for each spatial extent. The variance inflation factor was not included (NA) in the table for predictors that were removed due to multicollinearity (i.e., correlation coefficients > 0.7 or VIF > 3.0). Note that land area was not used for any of the analyses due to collinearity at three of the four spatial extents.

Predictor	**Cross-basin**	**Basin**	**Region**	**Sub-region**
Human population density within 50km (log)	1.76	1.49	1.33	1.32
Light attenuation (CV)	1.36	1.23	1.31	1.19
Light attenuation (mean)	2.36	2.09	1.41	1.45
Land area within 50km (log)	NA	NA	NA	1.41
Number of storms in past 30 years	1.29	1.20	1.18	1.03
Net primary productivity (CV)	1.35	1.30	1.25	1.11
Net primary productivity (mean)	1.91	1.22	1.30	1.18
Sea-surface temperature (CV)	2.15	2.35	1.53	1.41
Sea-surface temperature (mean)	NA	NA	1.67	1.28
Wave energy (CV)	1.12	1.11	1.27	1.26
Wave energy (mean)	1.83	1.28	1.44	1.32

Table S4. Bayesian P values for lack of fit between data simulated from posterior predictive distributions and observations for each scale of analysis. Extremely small Bayesian P values ($P <$ 0.05) indicate that the model predicted a smaller metric (e.g., the number of oases per grid cell) than observed in the data; extremely large Bayesian P values ($P < 0.95$) indicate that the model predicted a larger metric than observed in the data. Goodness of fit was evaluated using a Pearson χ^2 discrepancy metric for binomial data and a Freeman-Tukey discrepancy metric. The Pearson discrepancy was calculated as $\chi^2 = \sum_i \left(\frac{y_i - p_i n_i}{\sqrt{p_i n_i (1 - p_i)}}\right)^2$, where y_i is the observed number of oases, p_i is the estimated probability of detection, and n_i is the number of visits, in grid cell i. To avoid division by zero we added 0.001 to p_i in the denominator (Tobler et al. 2015, Kéry and Royle 2016). The Freeman-Tukey discrepancy was calculated as $\sum_i \left(\sqrt{y_i} - \sqrt{p_i\, n_i}\right)^2$.

Spatial extent	**Pearson χ^2**	**Freeman-Tukey**
Cross-basin	0.46	0.21
Basin	0.18	0.24
Region	0.12	0.20
Sub-region	0.15	0.13

Table S5. The direction of each predictor's coefficient at each spatial extent, along with the associated probability of the direction (i.e., the proportion of Markov chain iterations that were positive, or negative). Missing values (NA) in the table were for predictors that were removed due to multicollinearity (see Table S3), or for predictors whose coefficient switched from positive to negative at different spatial extents (e.g., mean wave energy). Coefficient of variation, CV.

Predictor	**Direction**	**Cross-basin**	**Basin**	**Region**	**Sub-region**
Human population density within 50km (log)	Negative	0.961	0.843	0.782	0.967
Light attenuation (CV)	Negative	0.598	NA	0.761	0.76
Light attenuation (CV)	Positive	NA	0.625	NA	NA
Light attenuation (mean)	Positive	0.891	1	1	1
Number of storms in past 30 years	Negative	0.846	0.566	0.579	NA
Number of storms in past 30 years	Positive	NA	NA	NA	0.559
Net primary productivity (CV)	Negative	0.715	0.773	0.611	0.819
Net primary productivity (mean)	Negative	0.607	NA	NA	NA
Net primary productivity (mean)	Positive	NA	0.728	0.692	0.595
Sea-surface temperature (CV)	Negative	0.875	0.846	NA	NA
Sea-surface temperature (CV)	Positive	NA	NA	0.995	0.886
Sea-surface temperature (mean)	Negative	NA	NA	NA	0.596
Sea-surface temperature (mean)	Positive	NA	NA	1	NA
Wave energy (CV)	Negative	0.967	0.796	0.595	NA
Wave energy (CV)	Positive	NA	NA	NA	0.797
Wave energy (mean)	Negative	0.601	NA	0.758	NA
Wave energy (mean)	Positive	NA	0.503	NA	0.624

Section S3: Supporting Figures

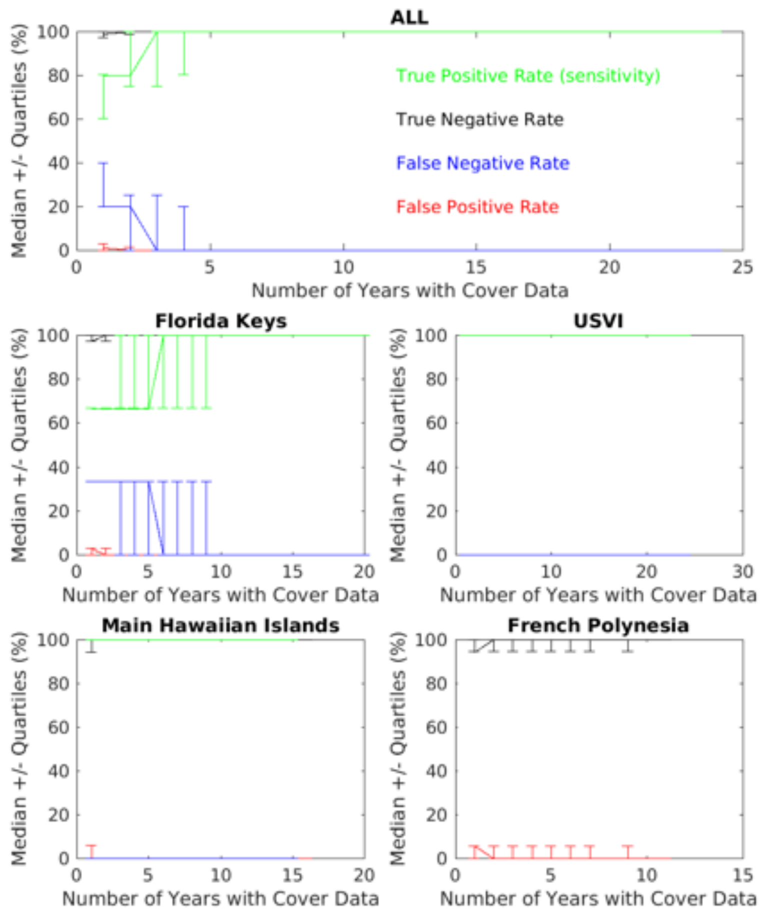

Figure S1. Results of simulations to understand the sensitivity of coral oasis designation to temporal replication (number of years with coral cover data), using time-series data from Guest et al. (2019). In all plots, the y-axis represents the median percent value (with upper and lower quartiles) of, for example, the true positive rate (green). That is, what percentage of simulations assigned each site the ‘true’ designation of an oasis, or not? The true designation is based on the complete time series of coral cover data within a region. We also include true negative, false negative, and false positive rates.

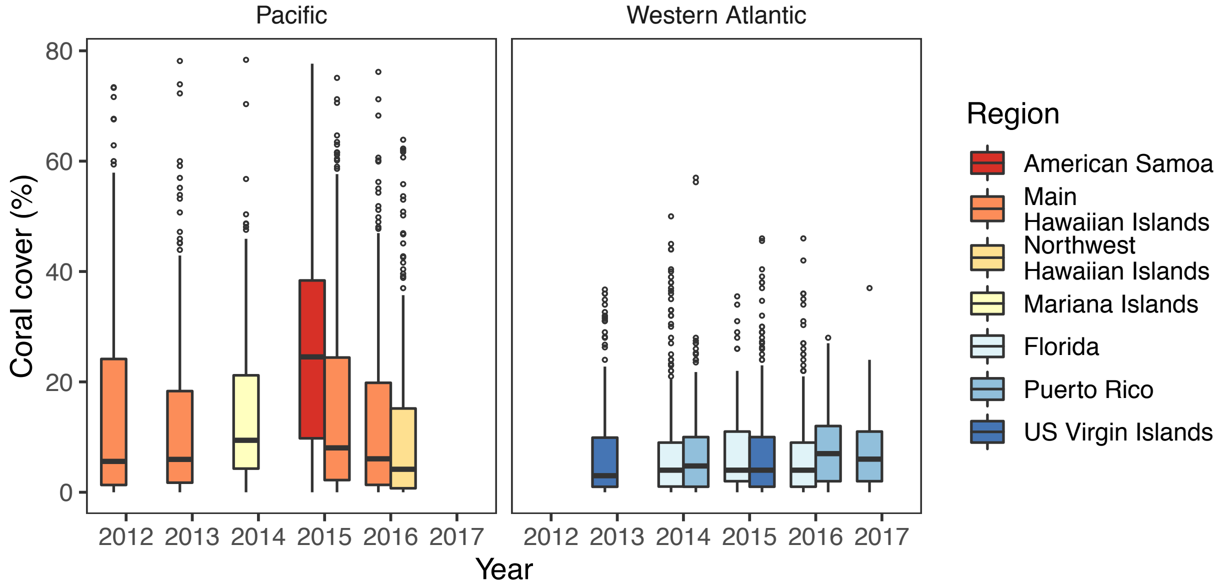

Figure S2. Patterns of coral cover (%) by year and region. Note that some regions were sampled only in a single year (e.g., American Samoa, Mariana Islands, Northwest Hawaiian Islands). Boxplots display the median and interquartile range (IQR) of data, with outliers plotted as circles beyond whiskers when the values are 1.5 × IQR from the first or third quartile.

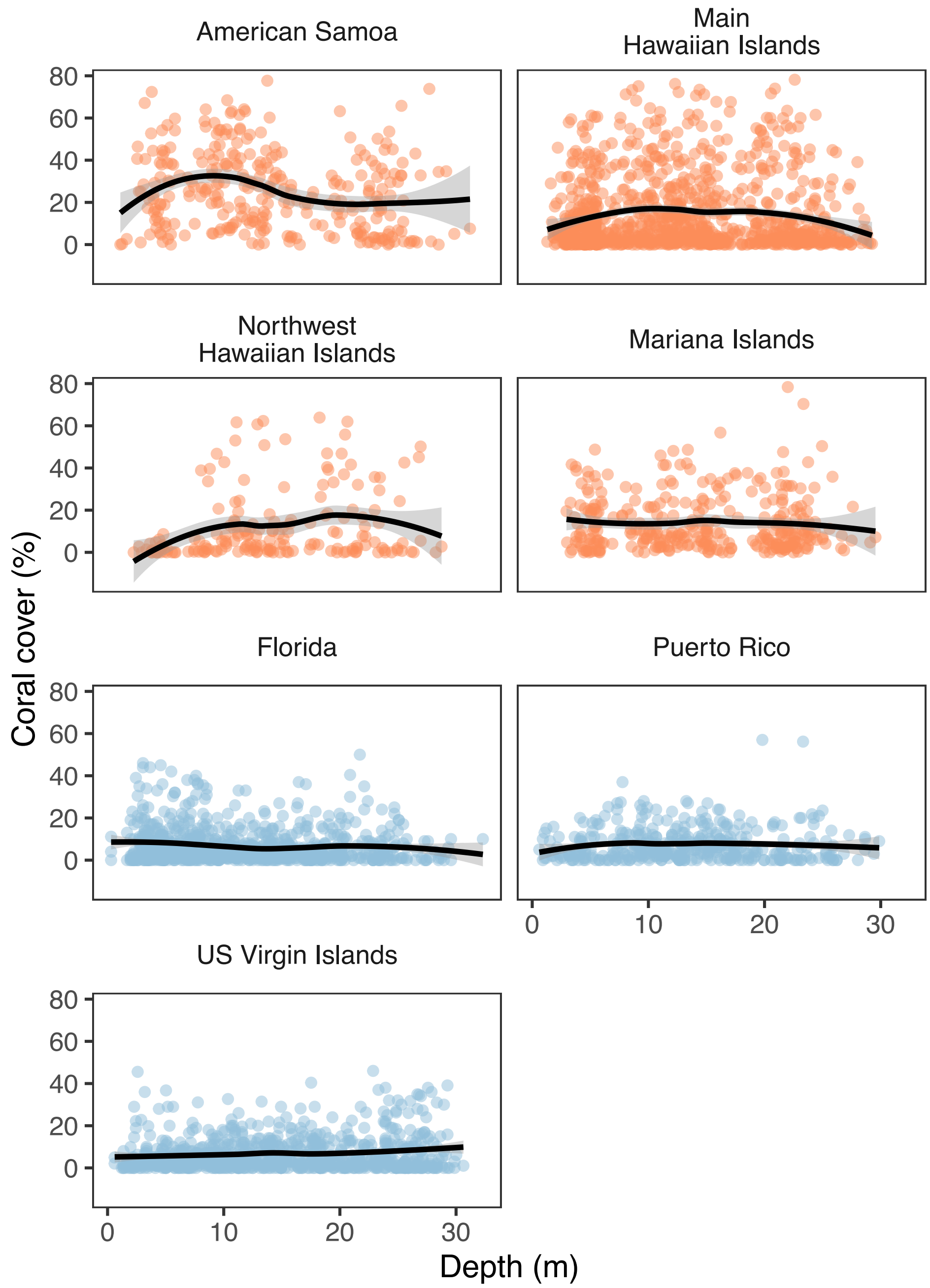

326

327 Figure S3. The relationship between coral cover (%) and depth (m) at the reef sites in each
328 region. The orange and blue points represent sites in the western Atlantic and Pacific basins,
329 respectively. The line represents a smoothed fit using a generalized additive model to illustrate
330 that there is no consistent effect of depth on coral cover.

331

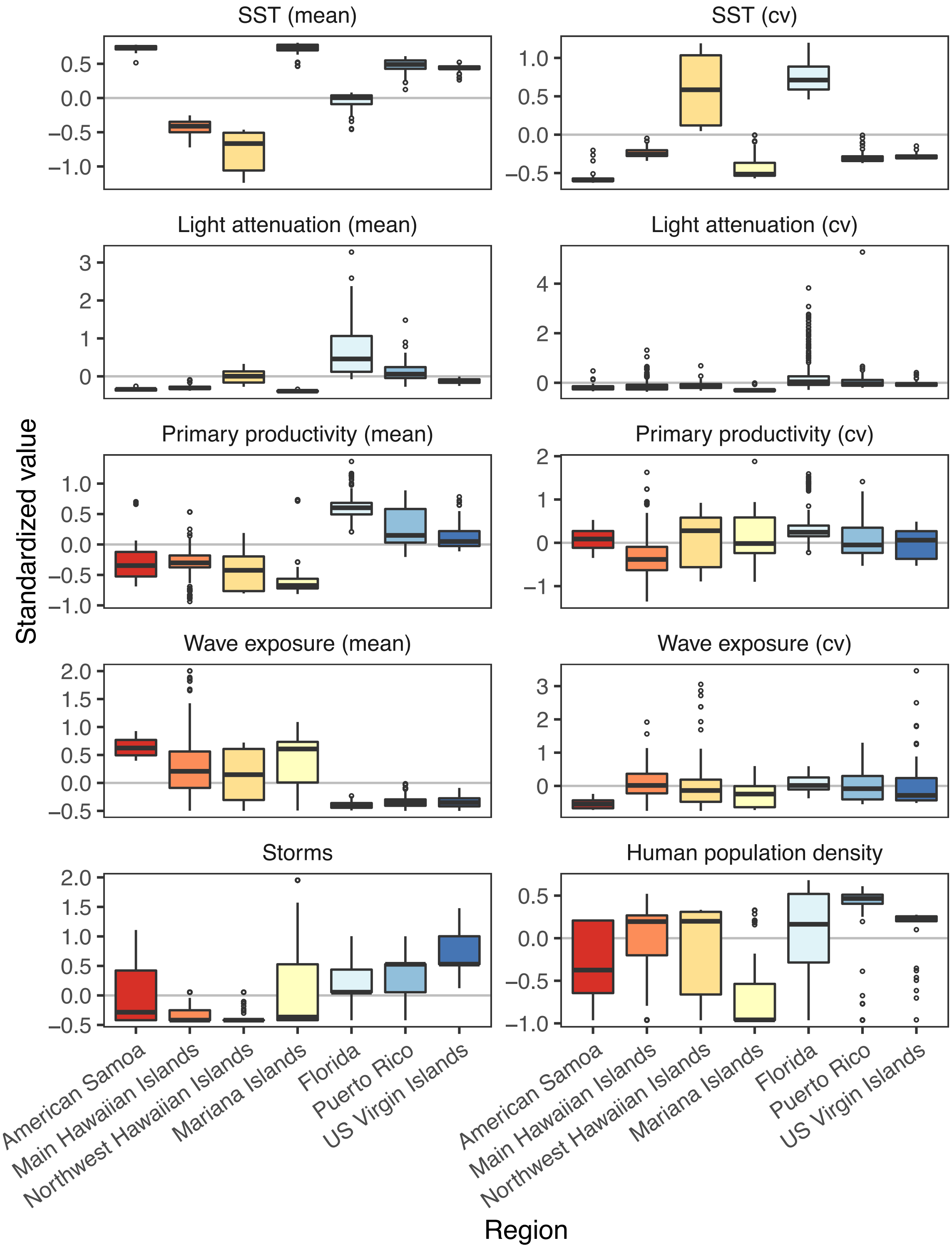

Figure S4. Distributions of covariates, standardized relative to the entire dataset (i.e., cross-basin extent). Boxplots display the median and interquartile range (IQR) of data, with outliers plotted as circles beyond whiskers when the values are 1.5 × IQR from the first or third quartile. Sea-surface temperature, SST; coefficient of variation, CV.

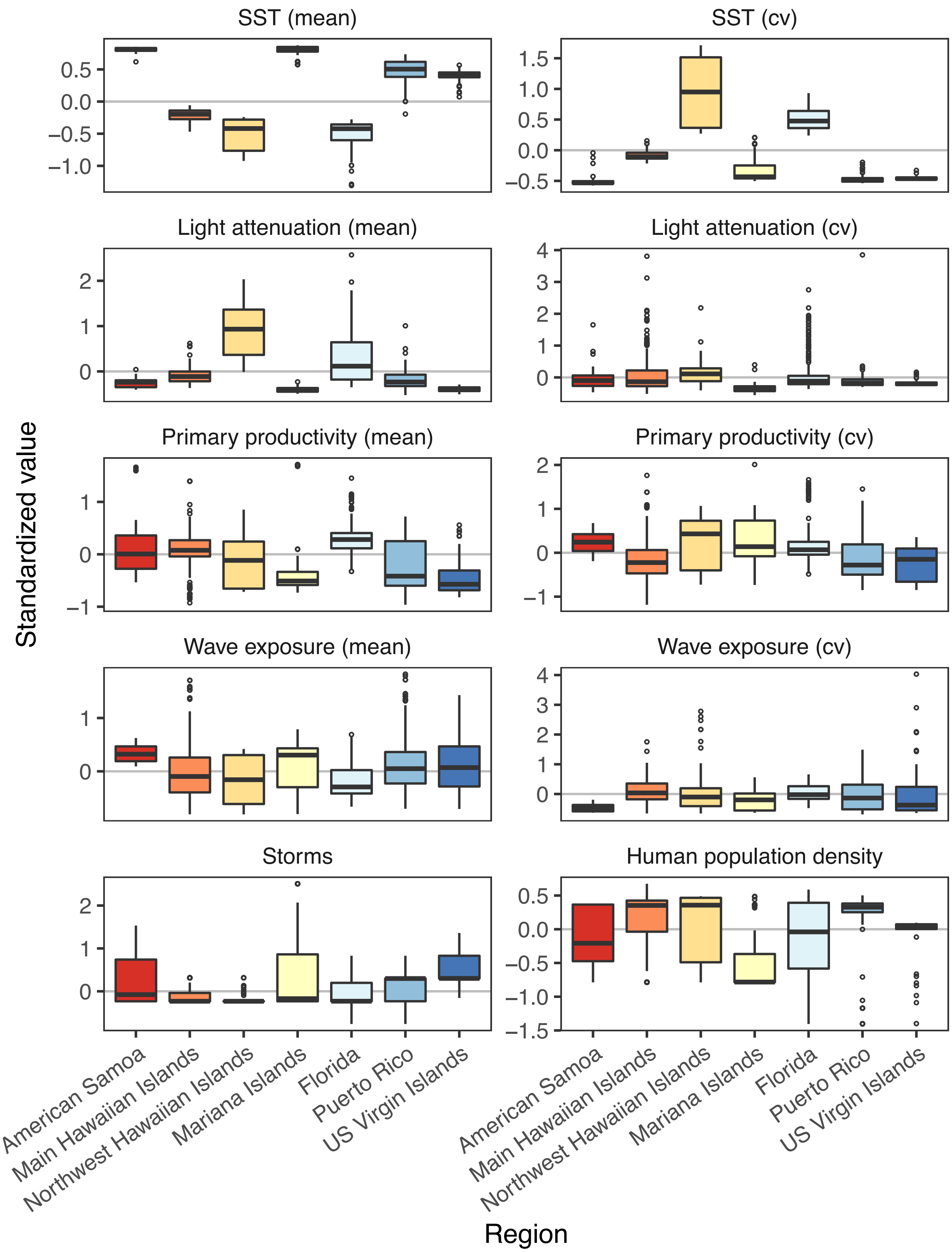

Figure S5. Distributions of covariates, standardized relative to each ocean basin (Pacific, western Atlantic). Boxplots display the median and interquartile range (IQR) of data, with outliers plotted as circles beyond whiskers when the values are 1.5 × IQR from the first or third quartile. Sea-surface temperature, SST; coefficient of variation, CV.

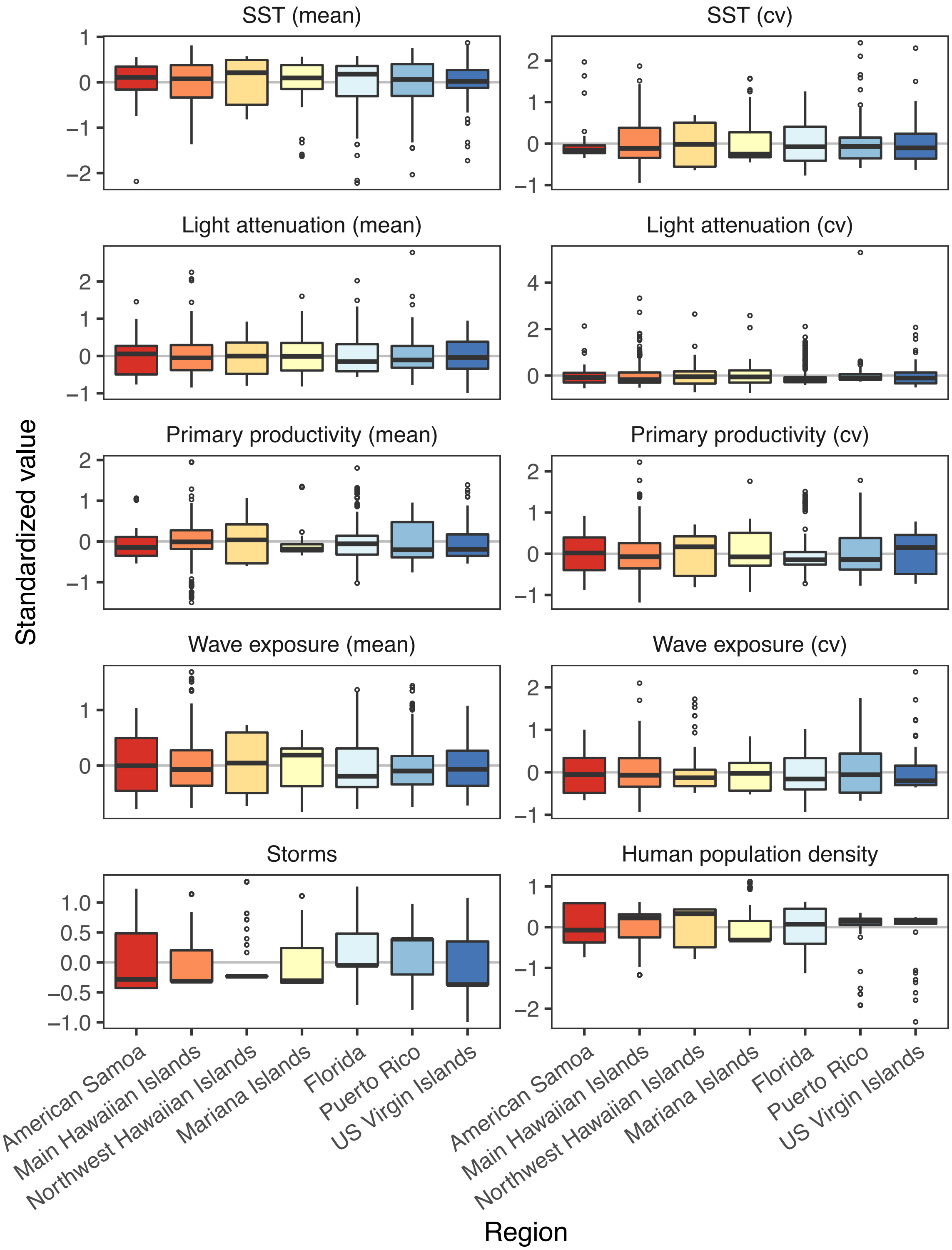

Figure S6. Distributions of covariates, standardized relative to each region. Boxplots display the median and interquartile range (IQR) of data, with outliers plotted as circles beyond whiskers when the values are 1.5 × IQR from the first or third quartile. Sea-surface temperature, SST; coefficient of variation, CV.

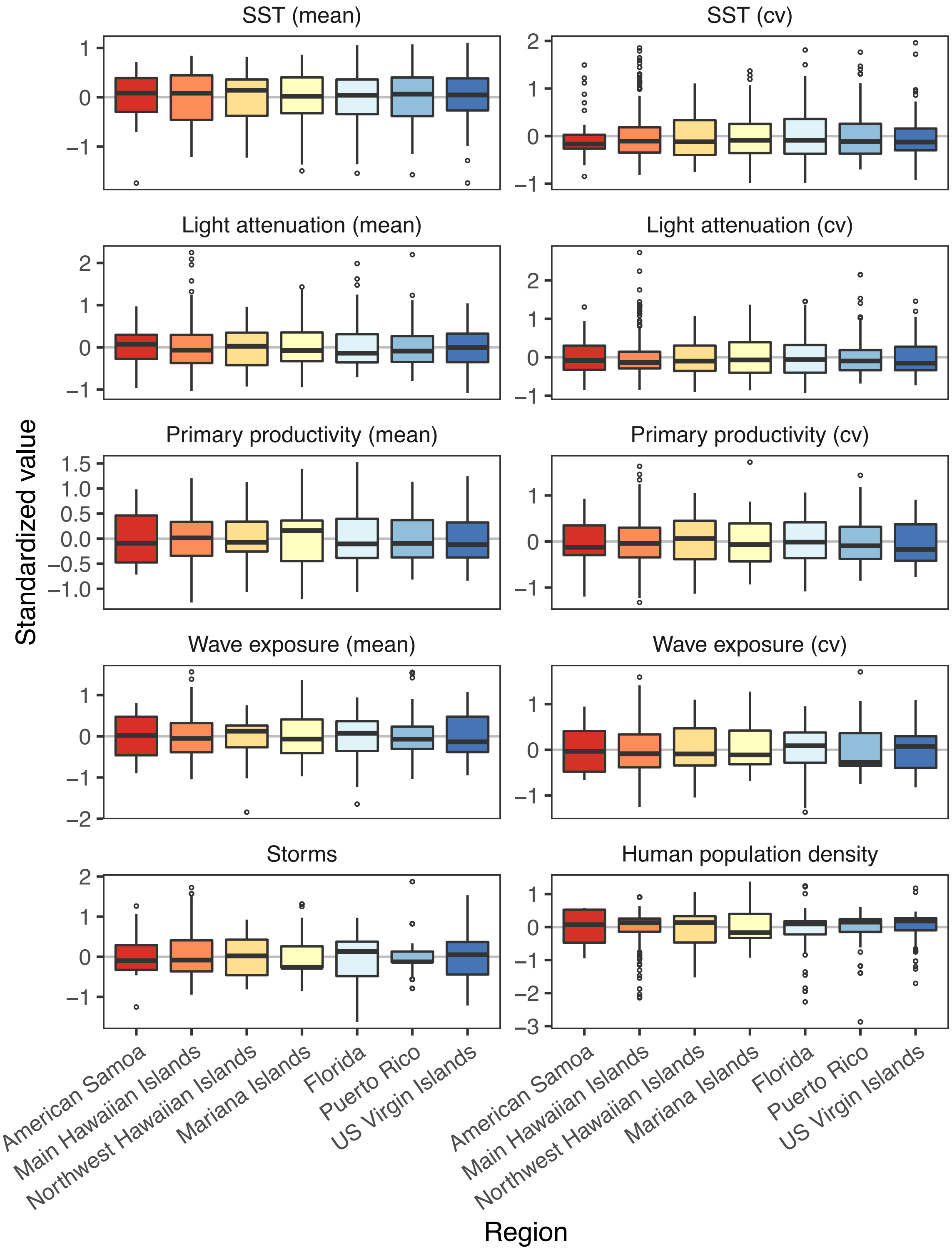

348
349 Figure S7. Distributions of covariates, standardized relative to each sub-region. Boxplots display
350 the median and interquartile range (IQR) of data, with outliers plotted as circles beyond whiskers

when the values are 1.5 × IQR from the first or third quartile. Sea-surface temperature, SST; coefficient of variation, CV.

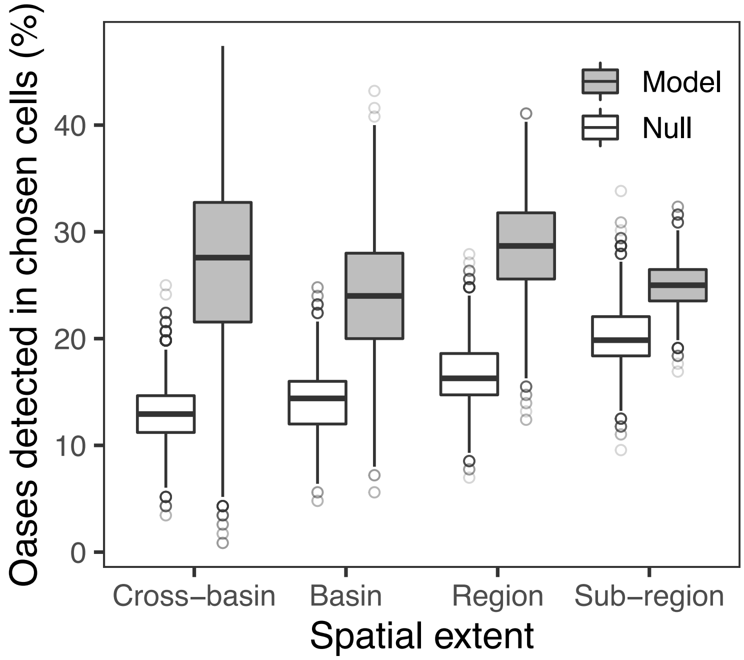

Figure. S8. The statistical model correctly identified a greater percentage of cells with detected coral oases than a null model at four spatial extents. See *Methods* for details. Boxplots display the median and interquartile range (IQR) of data, with outliers plotted as circles beyond whiskers when the values are 1.5 × IQR from the first or third quartile.

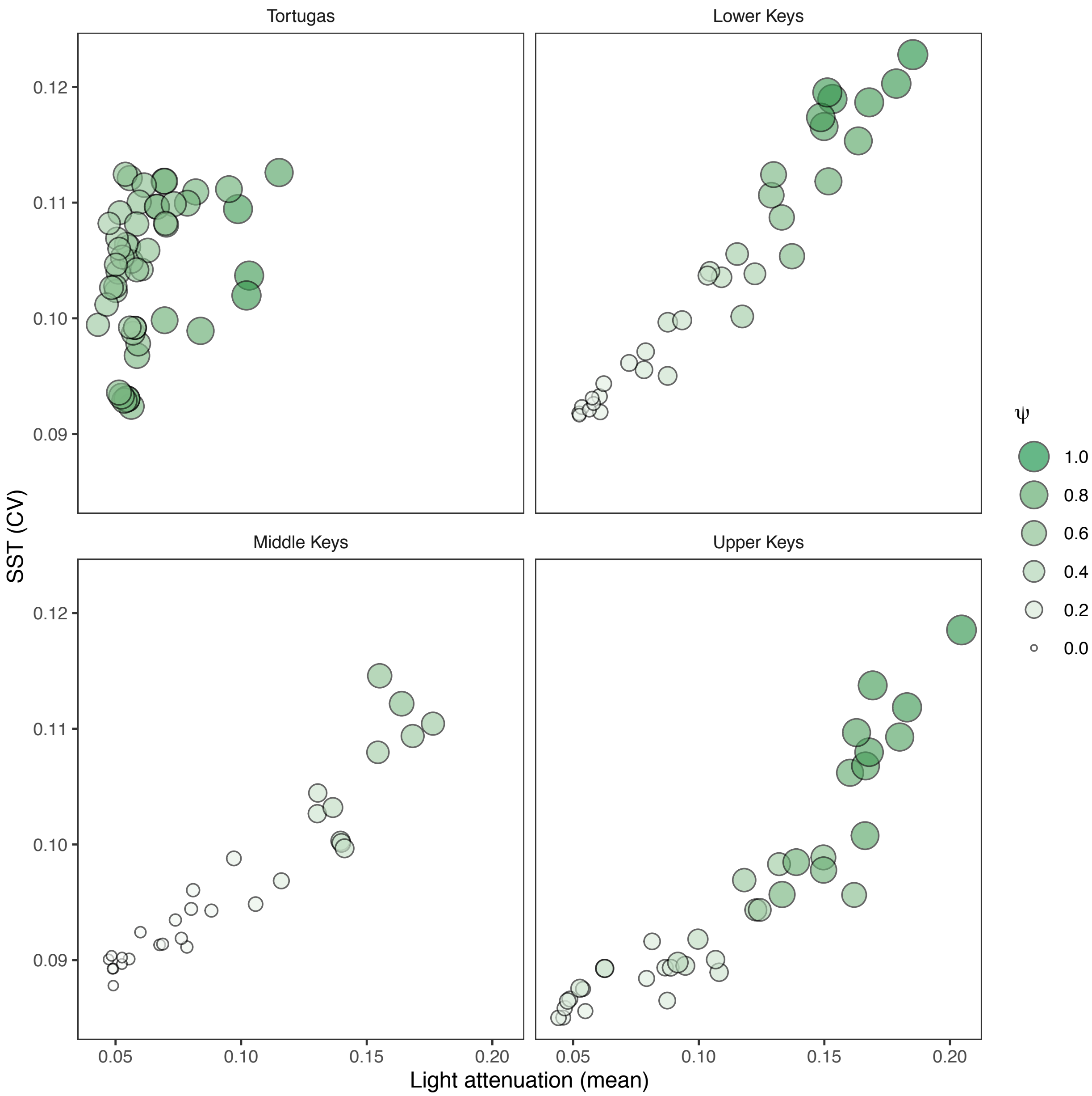

Figure S9. The relationship between mean light attenuation, the coefficient of variation (CV) in sea-surface temperature, and median predicted probability of oasis occurrence (ψ) at the regional extent in Florida (related to Figure 6).

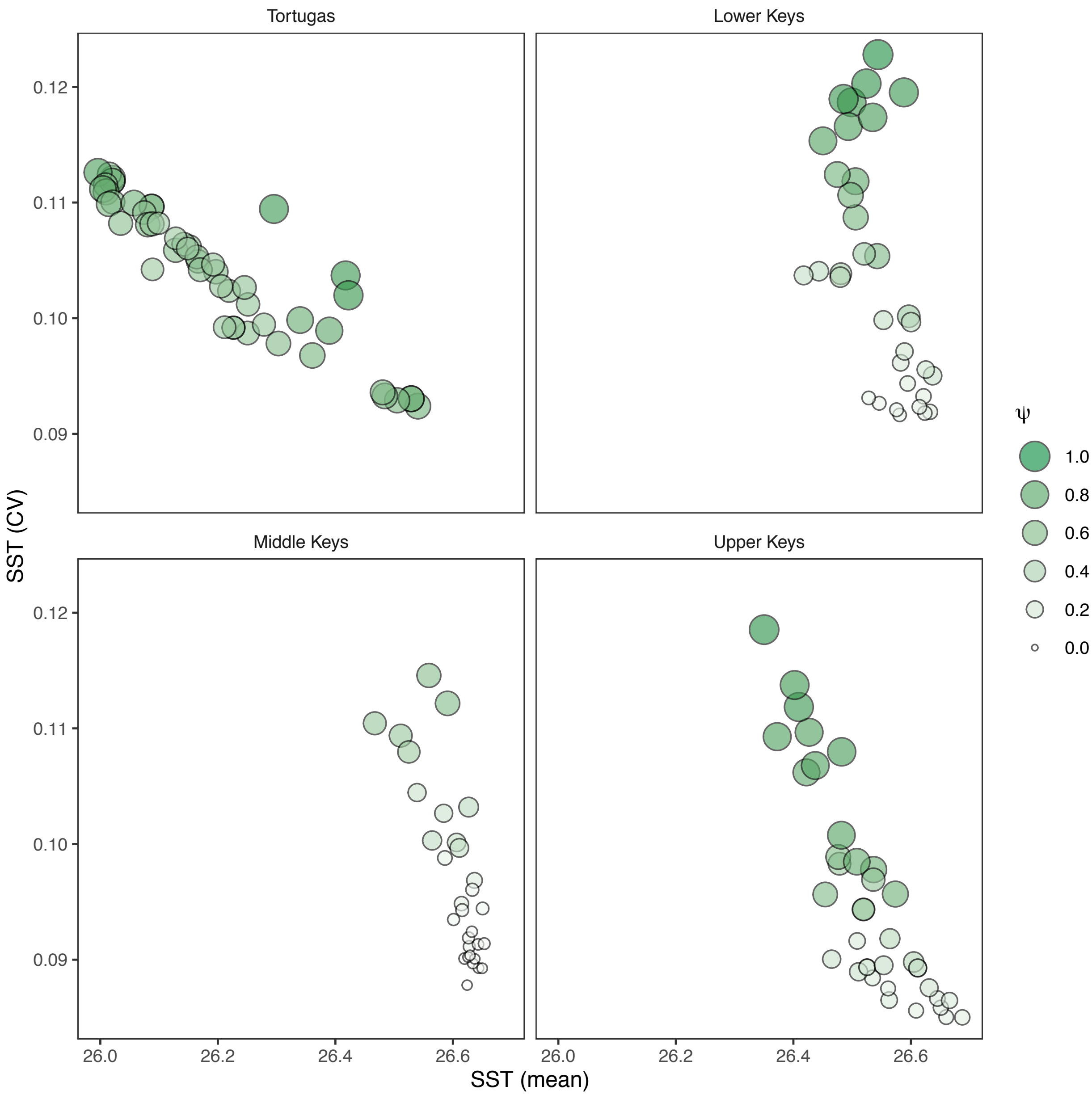

363

364 Figure S10. The relationship between mean sea-surface temperature (SST), the coefficient of

365 variation (CV) in SST, and median predicted probability of oasis occurrence (ψ) at the regional

366 extent in Florida (related to Figure 6).

Supporting References

Anthony, K., and P. Larcombe. 2000. Coral reefs in turbid waters: sediment-induced stresses in corals and likely mechanisms of adaptation. Pages 239-244 *in* Proceedings of the 9th International Coral Reef Symposium, Bali, Indonesia.

Barnes, B. B., C. Hu, B. A. Schaeffer, Z. Lee, D. A. Palandro, and J. C. Lehrter. 2013. MODIS-derived spatiotemporal water clarity patterns in optically shallow Florida Keys waters: A new approach to remove bottom contamination. Remote Sensing of Environment **134**:377-391.

Bruno, J. F., and A. Valdivia. 2016. Coral reef degradation is not correlated with local human population density. Scientific Reports **6**:29778.

Craig, P., C. Birkeland, and S. Belliveau. 2001. High temperatures tolerated by a diverse assemblage of shallow-water corals in American Samoa. Coral Reefs **20**:185-189.

Darling, E. S., T. R. McClanahan, J. Maina, G. G. Gurney, N. A. Graham, F. Januchowski-Hartley, J. E. Cinner, C. Mora, C. C. Hicks, and E. Maire. 2019. Social–environmental drivers inform strategic management of coral reefs in the Anthropocene. Nature Ecology & Evolution **3**:1341-1350.

Edmunds, P. J., and R. Elahi. 2007. The demographics of a 15-year decline in cover of the Caribbean reef coral *Montastraea annularis*. Ecological Monographs **77**:3-18.

Elsner, J. B., R. E. Hodges, and T. H. Jagger. 2012. Spatial grids for hurricane climate research. Climate Dynamics **39**:21-36.

Fitt, W., and M. Warner. 1995. Bleaching patterns of four species of Caribbean reef corals. The Biological Bulletin **189**:298-307.

Gardner, T. A., I. M. Cote, J. A. Gill, A. Grant, and A. R. Watkinson. 2005. Hurricanes and Caribbean coral reefs: impacts, recovery patterns, and role in long-term decline. Ecology **86**:174-184.

Guest, J. R., P. J. Edmunds, R. D. Gates, I. B. Kuffner, A. J. Andersson, B. B. Barnes, I. Chollett, T. A. Courtney, R. Elahi, K. Gross, E. A. Lenz, S. Mitarai, P. J. Mumby, H. R. Nelson, B. A. Parker, H. M. Putnam, C. S. Rogers, and L. T. Toth. 2018. A framework for identifying and characterising coral reef "oases" against a backdrop of degradation. Journal of Applied Ecology **55**:2865-2875.

Hughes, T. P. 1996. Demographic approaches to community dynamics: a coral reef example. Ecology **77**:2256-2260.

Kéry, M., and J. Royle. 2016. Applied hierarchical modelling in ecology—Modeling distribution, abundance and species richness using R and BUGS. 783 pages. Elsevier/Academic Press.

Kleypas, J. 1996. Coral reef development under naturally turbid conditions: fringing reefs near Broad Sound, Australia. Coral Reefs **15**:153-167.

Knapp, K. R., M. C. Kruk, D. H. Levinson, H. J. Diamond, and C. J. Neumann. 2010. The international best track archive for climate stewardship (IBTrACS) unifying tropical cyclone data. Bulletin of the American Meteorological Society **91**:363-376.

Lesser, M., W. Stochaj, D. Tapley, and J. Shick. 1990. Bleaching in coral reef anthozoans: effects of irradiance, ultraviolet radiation, and temperature on the activities of protective enzymes against active oxygen. Coral Reefs **8**:225-232.

Manzello, D. P., M. Brandt, T. B. Smith, D. Lirman, J. C. Hendee, and R. S. Nemeth. 2007. Hurricanes benefit bleached corals. Proceedings of the National Academy of Sciences **104**:12035-12039.

Marchand, P., and D. Gill. 2017. waver: Calculate Fetch and Wave Energy. R package version 0.2. 0.

McCoy, K., A. Heenan, J. M. Asher, P. Ayotte, K. Gorospe, A. E. Gray, K. Lino, J. P. Zamzow, and I. D. Williams. 2016. Pacific Reef Assessment and Monitoring Program. Data report: ecological monitoring 2015: reef fishes and benthic habitats of the main Hawaiian Islands, Northwestern Hawaiian Islands, Pacific Remote Island Areas, and American Samoa.

Mumby, P. J., J. R. Chisholm, A. J. Edwards, S. Andrefouet, and J. Jaubert. 2001. Cloudy weather may have saved Society Island reef corals during the 1998 ENSO event. Marine Ecology Progress Series **222**:209-216.

Nakamura, T., and R. van Woesik. 2001. Water-flow rates and passive diffusion partially explain differential survival of ocrals during the 1998 bleaching event. Marine Ecology Progress Series **212**:301-304.

Nyström, M. 2006. Redundancy and response diversity of functional groups: implications for the resilience of coral reefs. AMBIO: A Journal of the Human Environment **35**:30-35.

Oliver, T., and S. Palumbi. 2011. Do fluctuating temperature environments elevate coral thermal tolerance? Coral Reefs **30**:429-440.

Palumbi, S. R., D. J. Barshis, N. Traylor-Knowles, and R. A. Bay. 2014. Mechanisms of reef coral resistance to future climate change. Science **344**:895-898.

Puotinen, M. 2004. Tropical cyclones in the Great Barrier Reef, Australia, 1910–1999: a first step towards characterising the disturbance regime. Australian Geographical Studies **42**:378-392.

Robinson, D. 2019. fuzzyjoin: join tables together on inexact matching. R package version 0.1.5.

Robinson, J. P., I. D. Williams, L. A. Yeager, J. M. McPherson, J. Clark, T. A. Oliver, and J. K. Baum. 2018. Environmental conditions and herbivore biomass determine coral reef benthic community composition: implications for quantitative baselines. Coral Reefs **37**:1157-1168.

Safaie, A., N. J. Silbiger, T. R. McClanahan, G. Pawlak, D. J. Barshis, J. L. Hench, J. S. Rogers, G. J. Williams, and K. A. Davis. 2018. High frequency temperature variability reduces the risk of coral bleaching. Nature communications **9**:1-12.

Simpson, R. H., and H. Saffir. 1974. The hurricane disaster potential scale. Weatherwise **27**:169.

Smith, J. E., R. Brainard, A. Carter, S. Grillo, C. Edwards, J. Harris, L. Lewis, D. Obura, F. Rohwer, and E. Sala. 2016. Re-evaluating the health of coral reef communities: baselines and evidence for human impacts across the central Pacific. Proceedings of the Royal Society B: Biological Sciences **283**:20151985.

Sully, S., D. Burkepile, M. Donovan, G. Hodgson, and R. Van Woesik. 2019. A global analysis of coral bleaching over the past two decades. Nature communications **10**:1-5.

Sully, S., and R. van Woesik. 2020. Turbid reefs moderate coral bleaching under climate-related temperature stress. Global Change Biology.

Tobler, M. W., A. Zúñiga Hartley, S. E. Carrillo-Percastegui, and G. V. Powell. 2015. Spatiotemporal hierarchical modelling of species richness and occupancy using camera trap data. Journal of Applied Ecology **52**:413-421.

Treml, E., M. Colgan, and M. Keevican. 1997. Hurricane disturbance and coral reef development: a geographic information system (GIS) analysis of 501 years of hurricane data from the Lesser Antilles. Pages 541-546 *in* Proc 8th Int Coral Reef Symp.

Wall, M., L. Putchim, G. Schmidt, C. Jantzen, S. Khokiattiwong, and C. Richter. 2015. Large-amplitude internal waves benefit corals during thermal stress. Proceedings of the Royal Society B: Biological Sciences **282**:20140650.

Wessel, P., and W. H. Smith. 1996. A global, self-consistent, hierarchical, high-resolution shoreline database. Journal of Geophysical Research: Solid Earth **101**:8741-8743.

Williams, G. J., J. M. Gove, Y. Eynaud, B. J. Zgliczynski, and S. A. Sandin. 2015. Local human impacts decouple natural biophysical relationships on Pacific coral reefs. Ecography **38**:751-761.

Williams, I. D., C. S. Couch, O. Beijbom, T. A. Oliver, B. Vargas-Angel, B. D. Schumacher, and R. E. Brainard. 2019. Leveraging automated image analysis tools to transform our capacity to assess status and trends of coral reefs. Frontiers in Marine Science **6**.

Woodley, J., E. Chornesky, P. Clifford, J. Jackson, L. Kaufman, N. Knowlton, J. Lang, M. Pearson, J. Porter, and M. Rooney. 1981. Hurricane Allen's impact on Jamaican coral reefs. Science **214**:749-755.

Wyatt, A. S., J. J. Leichter, L. T. Toth, T. Miyajima, R. B. Aronson, and T. Nagata. 2020. Heat accumulation on coral reefs mitigated by internal waves. Nature Geoscience **13**:28-34.

Yeager, L. A., P. Marchand, D. A. Gill, J. K. Baum, and J. M. McPherson. 2017. Marine Socio-Environmental Covariates: queryable global layers of environmental and anthropogenic variables for marine ecosystem studies. Ecology **98**:1976-1976.

Zuur, A. F., E. N. Ieno, and C. S. Elphick. 2010. A protocol for data exploration to avoid common statistical problems. Methods in Ecology and Evolution **1**:3-14.